


ORIGINAL ARTICLE

Open Access



# Comparison of a deep learning-accelerated T2-weighted turbo spin echo sequence and its conventional counterpart for female pelvic MRI: reduced acquisition times and improved image quality

Jing Ren<sup>1</sup>, Yuan Li<sup>2</sup>, Fei-Shi Liu<sup>1</sup>, Chong Liu<sup>1</sup>, Jin-Xia Zhu<sup>3</sup>, Marcel Dominik Nickel<sup>4</sup>, Xiao-Ye Wang<sup>5</sup>, Xin-Yu Liu<sup>1</sup>, Jia Zhao<sup>1</sup>, Yong-Lan He<sup>1\*</sup> , Zheng-Yu Jin<sup>1\*</sup> and Hua-Dan Xue<sup>1\*</sup>

## Abstract

**Objectives:** To investigate the feasibility of a deep learning-accelerated T2-weighted turbo spin echo (TSE) sequence (T2<sub>DL</sub>) applied to female pelvic MRI, using standard T2-weighted TSE (T2<sub>S</sub>) as reference.

**Methods:** In total, 24 volunteers and 48 consecutive patients with benign uterine diseases were enrolled. Patients in the menstrual phase were excluded. T2<sub>S</sub> and T2<sub>DL</sub> sequences in three planes were performed for each participant. Quantitative image evaluation was conducted by calculating the signal-to-noise ratio (SNR) and contrast-to-noise ratio (CNR). Image geometric distortion was evaluated by measuring the diameters in all three directions of the uterus and lesions. Qualitative image evaluation including overall image quality, artifacts, boundary sharpness of the uterine zonal layers, and lesion conspicuity were assessed by three radiologists using a 5-point Likert scale, with 5 indicating the best quality. Comparative analyses were conducted for the two sequences.

**Results:** T2<sub>DL</sub> resulted in a 62.7% timing reduction (1:54 min for T2<sub>DL</sub> and 5:06 min for T2<sub>S</sub> in axial, sagittal, and coronal imaging, respectively). Compared to T2<sub>S</sub>, T2<sub>DL</sub> had significantly higher SNR ( $p \leq 0.001$ ) and CNR ( $p \leq 0.007$ ), and without geometric distortion ( $p = 0.925-0.981$ ). Inter-observer agreement regarding qualitative evaluation was excellent (Kendall's  $W > 0.75$ ). T2<sub>DL</sub> provided superior image quality (all  $p < 0.001$ ), boundary sharpness of the uterine zonal layers (all  $p < 0.001$ ), lesion conspicuity ( $p = 0.002$ ,  $p < 0.001$ , and  $p = 0.021$ ), and fewer artifacts (all  $p < 0.001$ ) in sagittal, axial, and coronal imaging.

**Conclusions:** Compared with standard TSE, deep learning-accelerated T2-weighted TSE is feasible to reduce acquisition time of female pelvic MRI with significant improvement of image quality.

\*Correspondence: heyonglan@pumch.cn; jin\_zhengyu@163.com; bjdanna95@hotmail.com

<sup>1</sup> Department of Radiology, Peking Union Medical College Hospital, Chinese Academy of Medical Sciences and Peking Union Medical College, Shuai Fu Yuan Road, Dongcheng Dist., Beijing 100730, People's Republic of China  
Full list of author information is available at the end of the article

## Key points

- $T_{2_{DL}}$  resulted in a 62.7% reduction in acquisition time compared to  $T_{2_S}$
- $T_{2_{DL}}$  can provide higher SNR and CNR, and without geometric distortion
- $T_{2_{DL}}$  is feasible for reducing the motion-induced blurring and improving image quality

**Keywords:** Magnetic resonance imaging, Female pelvis, Deep learning, Image quality, Turbo spin echo

## Introduction

Due to its excellent soft-tissue contrast, MRI is widely used to evaluate malignant and benign diseases of the female pelvis [1–3]. T2-weighted imaging (T2WI) is the standard sequence used in gynecological MRI and a basic female pelvic MRI protocol with at least two T2WI orthogonal planes is recommended for patients with uterine disease [1, 4, 5]. However, a disadvantage of traditional pelvic MR protocol is that it has a long acquisition time, ranging from approximately 10 to 15 min for T2w sequences, which may increase waiting time for patients and reduce throughput for medical centers [6–8]. In addition, the extensive duration of individual acquisitions renders the examination motion-sensitive, often resulting in motion artifacts or image blurring, especially in elderly patients or those with claustrophobia who are unable to remain still for long periods [9].

Multiple strategies have been employed to optimize acquisition of images in a limited timeframe while maintaining sufficient diagnostic value. Efforts to reduce motion artifacts include patient preparation (e.g., use of an intravenous antiperistaltic agent, fasting, or emptying of the bladder) and scanning techniques (e.g., fat suppression, saturation bands, or signal averaging). However, these methods do not completely eradicate artifacts and may increase the cost and duration of MR examinations [5, 10, 11]. Innovative techniques that may substantially reduce scanning time while producing motion-resistant images include partial Fourier acquisition, parallel acquisition techniques, and compressed sensing (CS). Partial Fourier imaging and parallel acquisition techniques are time-saving technologies that omit phase-encoding steps in a regular fashion, but lead to SNR loss [11, 12]. CS requires an incoherent undersampling pattern; however, the images exhibit residual blurring and an unnatural appearance due to oversimplified image content [13, 14]. Although these sequences are routinely available, their clinical use is limited because of trade-offs between saving time and loss of SNR, sharpness, or natural appearance [13, 15].

With recent advances in artificial intelligence, a deep learning (DL) reconstruction method involving an unrolled variational network allows for a reduction in

acquisition time while preserving image quality and realistic textures [16]. The particular feature of unrolled variational networks in the DL algorithm beyond image denoising is given by the fact that the network constantly considers data consistency with the acquired k-space data through a parallel imaging model. This allows to reduce the noise significantly and provide images with higher SNR [17]. It is therefore possible to invest the potential improvement in shorting of the acquisition time by employing higher acceleration factors or fewer averages. Previous studies have found that the DL algorithm enables to yield satisfactory image quality and significantly save time in MRI protocols for the abdomen, knee, and prostate (DL vs. conventional sequences: 0:16 vs. 4:00 min, 4:20 vs. 8:11 min, and 1:38–3:50 vs. 4:37–10:21 min, respectively) [17–20]. However, the value of DL-accelerated reconstruction technique applied to female pelvic MRI has not been studied. We hypothesized that this DL reconstruction method would accelerate the gynecological MRI protocol while producing high-quality images. To test this hypothesis, we compared the feasibility of the DL-accelerated TSE sequence ( $T_{2_{DL}}$ ) with that of a standard TSE sequence ( $T_{2_S}$ ) for gynecological T2WI by evaluating examination time, image quality, and lesion conspicuity of benign uterine diseases.

## Methods

### Study design

This prospective study was approved by our institutional review board and complied with ethical committee standards. The sample size was estimated by considering both the difference in quantitative parameter means (using paired t-test/Wilcoxon signed-rank test) or qualitative evaluation scores (using Wilcoxon signed-rank test) between the DL-accelerated turbo spin echo (TSE) sequence ( $T_{2_{DL}}$ ) and standard T2-weighted TSE sequence ( $T_{2_S}$ ). Sample size estimation was conducted using G\*Power 3 (version 3.1.9.7), and the statistical test was set as “matched pairs—different between two dependent means/Wilcoxon signed-rank test”. The error was set at 0.05, and the power level was set to 80–95%. Therefore, a total sample size of 22–38 was estimated when considering the difference in quantitative

parameter means between  $T2_{DL}$  and  $T2_S$ , while a sample size of 23–39 was obtained when considering the difference in qualitative evaluation score between  $T2_{DL}$  and  $T2_S$ . The latter was selected as the target sample size for the study because it was larger. Then, participants in the study were enrolled in two stages: volunteers enrolled for feasibility evaluation and patients enrolled for clinical application (Fig. 1). Considering that  $T2_{DL}$  has not been used in female pelvic MRI before, we firstly recruited 24 healthy female volunteers who had no contraindications for MRI between May 2021 and July 2021 to preliminarily explore the feasibility of  $T2_{DL}$ . Then, between August 2021 and December 2021, a totally of 48 consecutive female patients who underwent pelvic MRI for indications of benign uterine disease were enrolled (Table 1). Participants in the menstrual phase were excluded as boundary sharpness of the uterine zonal layers is reduced in this phase [21]. Written informed consent was obtained from participants.

**MRI technique**

Participants received a 10-mL glycerin enema in the rectum 30 min before MRI to reduce air in the rectum

**Table 1** Characteristics of the study population

Characteristics	
Total (n. %)	72 (100)
Age (years)	35.50 (25.25–42.75)
BMI (kg/cm <sup>2</sup> )	21.58 (19.73–23.81)
Volunteers (n. %)	24 (33)
Age (year)	25.00 (24.00–26.75)
BMI (kg/cm <sup>2</sup> )	19.73 (18.62–21.51)
Patients (n. %)	48 (67)
Age (year)*	39.81 ± 8.95
BMI (kg/cm <sup>2</sup> )	22.77 (21.25–24.15)
Disease (n. %)	
Leiomyoma	27 (56)
Adenomyosis	9 (19)
Scarred uterus	12 (25)

BMI, body-mass index

\*Continuous variables conforming to a normal distribution are presented as means ± standard deviations- otherwise as median (interquartile range [IQR])

and sigmoid. A moderately full bladder was required [5]. MRI studies were performed using a 3 T MR system (MAGNETOM Vida, Siemens Healthcare, Erlangen,

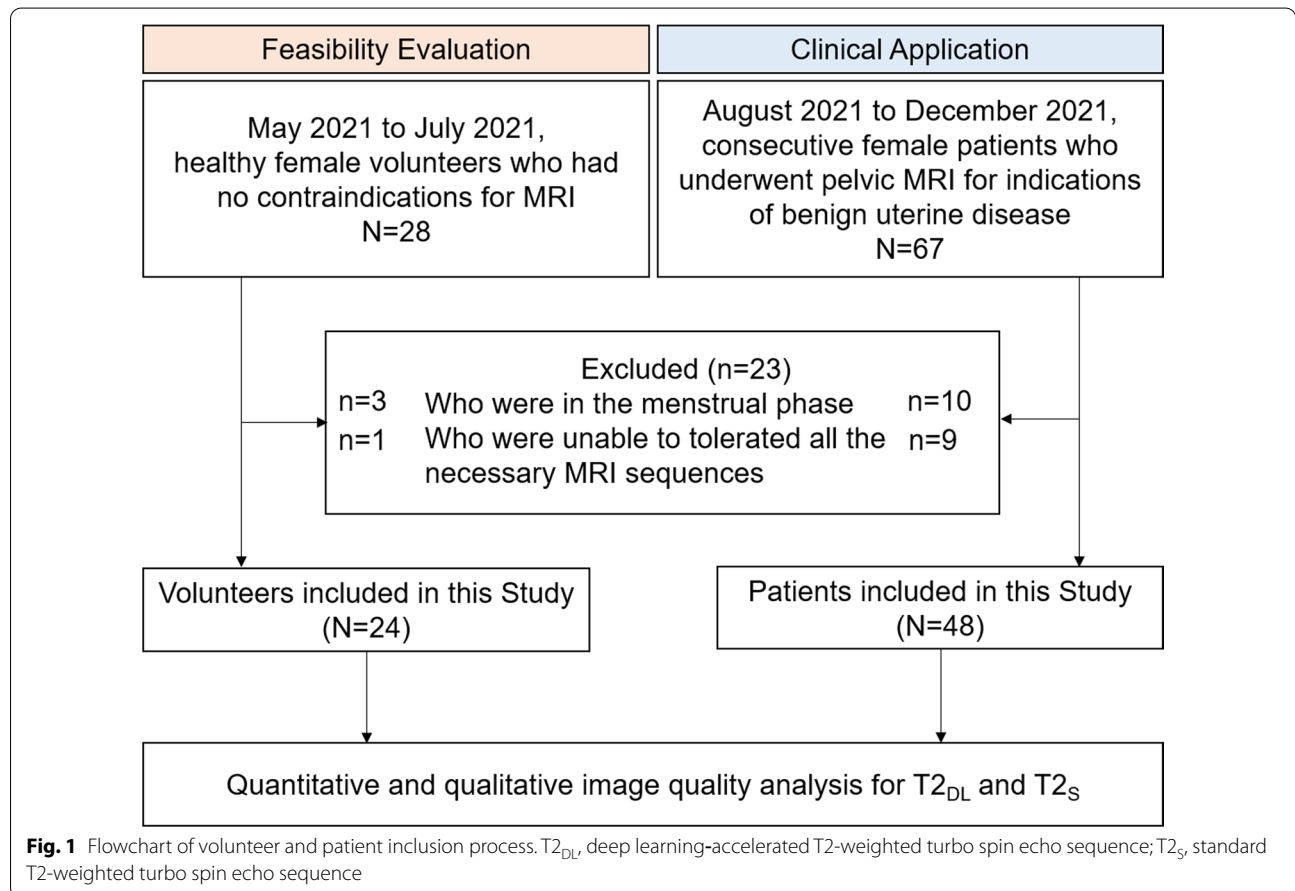


**Fig. 1** Flowchart of volunteer and patient inclusion process.  $T2_{DL}$ , deep learning-accelerated T2-weighted turbo spin echo sequence;  $T2_S$ , standard T2-weighted turbo spin echo sequence

Germany) with an 18-channel body phased-array receive coil. Unenhanced female pelvic MR protocol was performed using the following sequences: standard T2-weighted TSE sequence ( $T2_S$ ) in axial, sagittal, and coronal planes; T2WI acquired with a prototypic DL-accelerated TSE sequence ( $T2_{DL}$ ) (Siemens Healthcare, Erlangen, Germany) in axial, sagittal, and coronal planes; axial T1-weighted imaging (T1WI); and DWI with two  $b$  values in the axial plane (50 and 800 s/mm<sup>2</sup>).  $T2_{DL}$  was acquired after  $T2_S$  to ensure the standard-of-care practice for clinical MRI. The detailed parameters for both T2W protocols are listed in Table 2.

### Quantitative image evaluation

All axial, sagittal, and coronal T2W images ( $T2_S$  and  $T2_{DL}$ ) were randomized, anonymized, and independently evaluated using image-viewing software (RadiAnt DICOM Viewer 2020.1). Quantitative image evaluation was performed by a radiologist with 3 years of experience interpreting pelvic MR images. Whenever possible, operator-defined ROIs were placed on sagittal T2w images in the myometrium, junctional zone, gluteal muscle, and leiomyoma. The ROIs were as large as possible and were devoid of severe artifacts. The ROIs in the gluteal muscle were relatively small because care was taken to avoid areas of macroscopic fat.

The SD of the background signal intensity (SI) of images was measured as the noise value. The SNR for the myometrium, junctional zone, and leiomyoma is calculated according to Eq. 1 [22, 23]:

$$\text{SNR} = \frac{\text{SI}}{N} \quad (1)$$

**Table 2** Detail T2-weighted MR imaging parameters for  $T2_{DL}$  and  $T2_S$  sequences

	Sagittal / Axial / Coronal	
	$T2_{DL}$	$T2_S$
Repetition time (ms)	3000	3000
Echo time (ms)	95	95
Field of view (mm <sup>2</sup> )	200 × 200	200 × 200
Matrix	432 × 367	432 × 367
Slice thickness (mm)	4	4
No. of slices	28	28
Reconstructed voxel size (mm <sup>3</sup> )	0.2 × 0.2 × 4.0	0.2 × 0.2 × 4.0
Parallel acceleration factor	3	3
Averages	1	2
Acquisition time (min:sec)	1:54	5:06

$T2_{DL}$  deep learning-accelerated T2-weighted turbo spin echo sequence;  $T2_S$  standard T2-weighted turbo spin echo sequence

where SI is the mean SI within the ROIs, and N is the background noise. The CNR was then determined between the (1) myometrium and junctional zone, (2) myometrium and gluteal muscle, (3) junctional zone and gluteal muscle, and (4) myometrium and leiomyoma, according to Eq. 2 [22; 23]:

$$\text{CNR} = \frac{\text{SI}_A - \text{SI}_B}{N}, \quad (2)$$

where  $\text{SI}_A$  and  $\text{SI}_B$  are the mean SIs of the two tissue types mentioned previously. Care was taken to size and place the ROIs consistently for each pair of images from the same patient. In patients with multiple lesions, only the largest lesions were analyzed.

Geometric image distortion was evaluated by measuring the diameters in all three directions of the uterus and lesions depicted on both  $T2_{DL}$  and  $T2_S$  images. For the 24 healthy volunteers, the long (i.e., parallel to the long axis of the uterine body), short (i.e., maximum length perpendicular to the long diameter), and transverse (i.e., distance between the two uterine horns) diameters of the uterus were measured on both  $T2_{DL}$  and  $T2_S$  slices in which the uterus appeared largest. Given the relative ease and accuracy of uterine leiomyoma as compared to adenomyosis and scarred uterus measurements, for each affected patient ( $n=27$ ),  $T2_{DL}$  and  $T2_S$  slices with the maximum lesion area were examined for the largest lesion, followed by measurements of the anteroposterior, vertical, and transverse diameters of this lesion.

### Qualitative image evaluation

All anonymized image datasets were independently evaluated in a random order by three radiologists with 3, 5, and 11 years of experience in interpreting pelvic MR images. The readers were blinded to the sequence types, as image information was concealed in the viewing software. Overall image quality, artifacts, boundary sharpness of the uterine zonal layers, and lesion conspicuity on axial, coronal, and sagittal images were rated by the radiologists using a 5-point Likert scale, with 1 and 5 representing the poorest and best performance, respectively (Table 3). In patients with multiple lesions, only a single score was assigned after the consideration of all lesions.

### Statistical analysis

Statistical analysis was performed using SPSS version 21.0.0.0 (IBM; <https://www.ibm.com>). After testing for normality using the Kolmogorov–Smirnov test, continuous variables conforming to a normal distribution are presented as means ± standard deviations, otherwise as median (interquartile range [IQR]). Ordinal scaled variables are presented as median (IQR). The results of quantitative analysis were compared using a paired  $t$ -test for

**Table 3** Qualitative image evaluations based on the 5-point Likert scale

Score	Overall image quality	Artifacts	Boundary sharpness of the uterine zonal layers	Lesion conspicuity
1	Non-diagnostic	Non-diagnostic	Unable to see	Lesion unidentifiable
2	Substantial deficits in image quality	Substantial impact on diagnosis	Blurry but visualized	No differentiation between lesion and normal anatomy
3	Moderate image quality	Moderate impact on diagnosis	Acceptable	Subtle lesion with poorly defined edges
4	Good image quality	Little impact on image diagnosis	Good	Well-seen lesion with poorly defined edges
5	Excellent image quality	No artifact	Excellent	Well-seen lesion with well-defined edges

normally distributed variables, or Wilcoxon signed-rank test for nonnormally distributed variables. The distribution and concordance of uterine and lesion diameters in all three directions were obtained on both T2<sub>DL</sub> and T2<sub>S</sub> images and were presented in Bland–Altman plots. Qualitative scores were compared using the Wilcoxon signed-rank test. Interobserver agreement was evaluated using the Kendall W test ( $\leq 0.4$ , poor agreement; 0.41–0.75, good agreement;  $> 0.75$ , excellent agreement). Two-tailed  $p$  values  $< 0.05$  were considered statistically significant.

## Results

### Patient characteristics

In total, 72 participants (median [IQR] age: 35.50 [25.25–42.75] years; range: 23–71 years) were included in this study. The body mass index of participants was 21.58 (19.73–23.81) kg/cm<sup>2</sup> (range: 16.94–37.20 kg/m<sup>2</sup>). Among the 48 patients with benign pelvic diseases, 27 had uterine leiomyoma, 9 had adenomyosis, and 12 had a scarred uterus.

### Quantitative image evaluation

The acquisition time of axial, sagittal, and coronal imaging was 1:54 min and 5:06 min for T2<sub>DL</sub> and T2<sub>S</sub>, respectively. The total acquisition time, including all T2-weighted sequences, was 5:42 min and 15:18 min for T2<sub>DL</sub> and T2<sub>S</sub>, respectively. Overall, the acquisition time of T2<sub>DL</sub> images was reduced by 62.7% compared to that of T2<sub>S</sub> images. A total of 432 image datasets were independently evaluated. The median (IQR) or mean  $\pm$  SD areas of ROIs in the myometrium, junctional zone, gluteal muscle, leiomyoma, and image background were 69.10 (52.83–76.93) mm<sup>2</sup>, 11.30 (8.10–17.65) mm<sup>2</sup>, 25.51  $\pm$  10.69 mm<sup>2</sup>, 579.75 (153.70–1286.73) mm<sup>2</sup>, and 1052.03  $\pm$  586.69 mm<sup>2</sup>, respectively. The mean SNRs of the myometrium, junctional zone, and leiomyoma were significantly higher on T2<sub>DL</sub> images than on T2<sub>S</sub> images (108.63 vs. 76.36,  $p < 0.001$ ; 57.64 vs. 40.77,  $p < 0.001$ ; and 44.98 vs. 32.86,  $p = 0.001$ , respectively) (Fig. 2a). The mean CNRs were also significantly higher on T2<sub>DL</sub> images than on T2<sub>S</sub> images: between the myometrium and junctional zone, 60.14 vs. 42.32,  $p < 0.001$ ; between

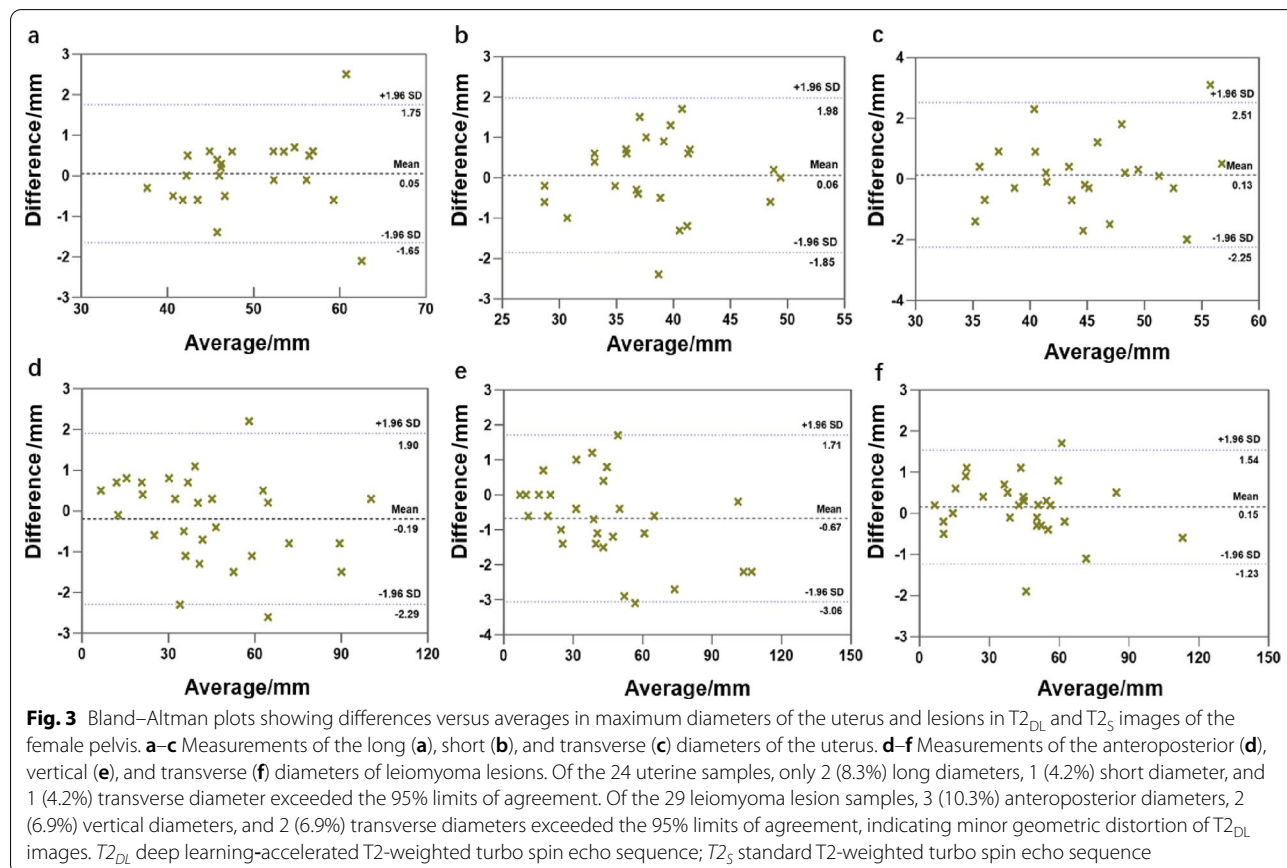
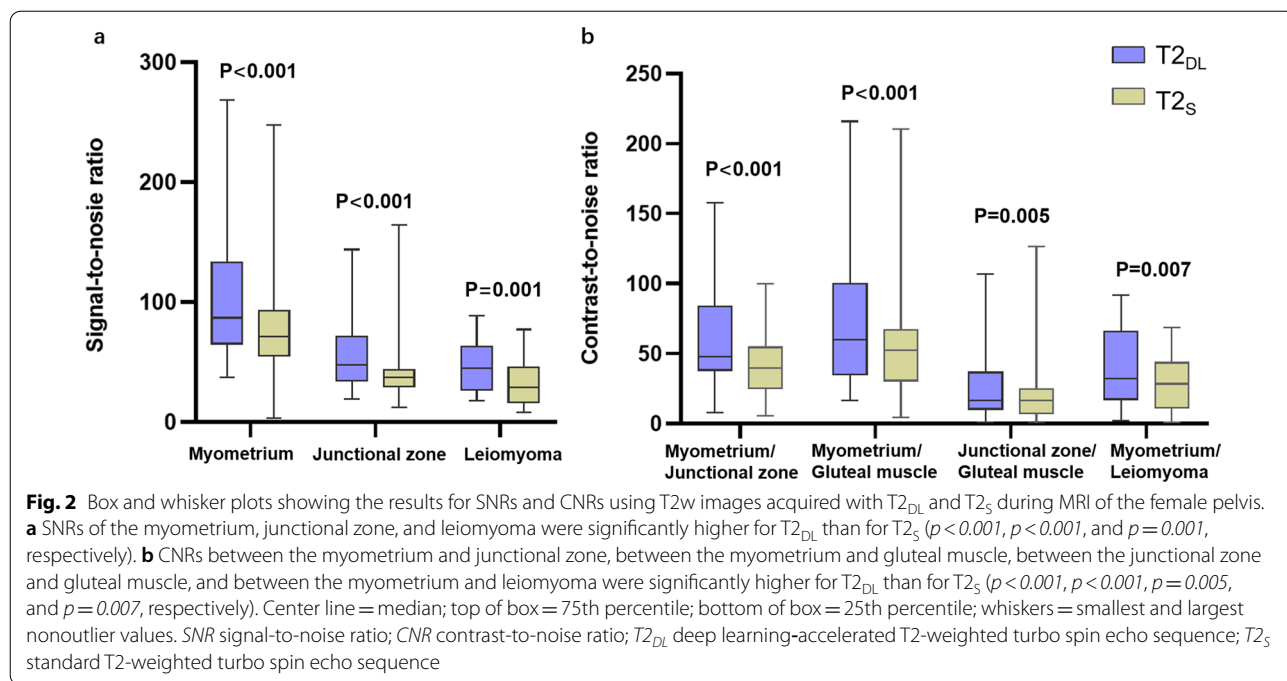
the myometrium and gluteal muscle, 76.43 vs. 54.73,  $p < 0.001$ ; between the junctional zone and gluteal muscle, 25.63 vs. 19.47,  $p = 0.005$ ; and between the myometrium and leiomyoma, 39.13 vs. 28.29,  $p = 0.007$  (Fig. 2b).

Quantitative measurements revealed no significant differences in maximum diameter of the uterus and leiomyoma lesions between the two sequences. Mean  $\pm$  SD long, short, and transverse diameters of the uterine body were 49.29  $\pm$  7.03 mm, 38.27  $\pm$  5.58 mm, and 44.92  $\pm$  6.39 mm, respectively, for T2<sub>DL</sub> and 49.23  $\pm$  6.89 mm, 38.20  $\pm$  5.54 mm, and 44.80  $\pm$  6.23 mm, respectively, for T2<sub>S</sub> ( $p = 0.979$ ,  $p = 0.969$ , and  $p = 0.944$ , respectively). The mean  $\pm$  SD anteroposterior, vertical, and transverse diameters of the leiomyoma lesions were 44.22  $\pm$  23.87 mm, 43.37  $\pm$  26.65 mm, and 44.28  $\pm$  23.51 mm, respectively, for T2<sub>DL</sub> and 44.41  $\pm$  24.17 mm, 44.04  $\pm$  27.17 mm, and 44.12  $\pm$  23.63 mm, respectively, for T2<sub>S</sub> ( $p = 0.976$ ,  $p = 0.925$ , and  $p = 0.981$ , respectively). Bland–Altman plots revealed minimal geometric distortion in the T2<sub>DL</sub> images. The mean difference in percentage and limits of agreement between T2<sub>DL</sub> and T2<sub>S</sub> was  $-0.67\%$  to 0.15% (Fig. 3).

### Qualitative image evaluation

Interobserver agreement on qualitative image evaluation among the three readers was excellent (Kendall W coefficient: 0.801–0.903 for T2<sub>DL</sub> and 0.771–0.914 for T2<sub>S</sub>; all  $p < 0.001$ ). Images from 72 participants were used to evaluate the overall image quality, artifacts, and boundary sharpness of the uterine zonal layers and images from 37 patients with visible lesions were used to evaluate lesion conspicuity. The overall quality of sagittal, axial, and coronal images was rated higher for T2<sub>DL</sub> (median [IQR] of 5 (4–5), 5 (4–5), and 5 (4–5), respectively) than for T2<sub>S</sub> (median [IQR] of 4 (4–5), 4 (4–4), and 4 (4–4); all  $p < 0.001$ ).

Ghost artifacts were detected in T2<sub>S</sub> images from all patients. Artifacts were also observed in T2<sub>DL</sub> images, but they were significantly reduced in some sagittal, axial, and coronal images (median [IQR] scores for T2<sub>S</sub> and T2<sub>DL</sub> were 4 [4–5] and 5 [4–5], 4 [4–5] and 5 [5–5], and 4 [4–5] and 5 [4–5], respectively, all  $p < 0.001$ ) (Figs. 4, 5,



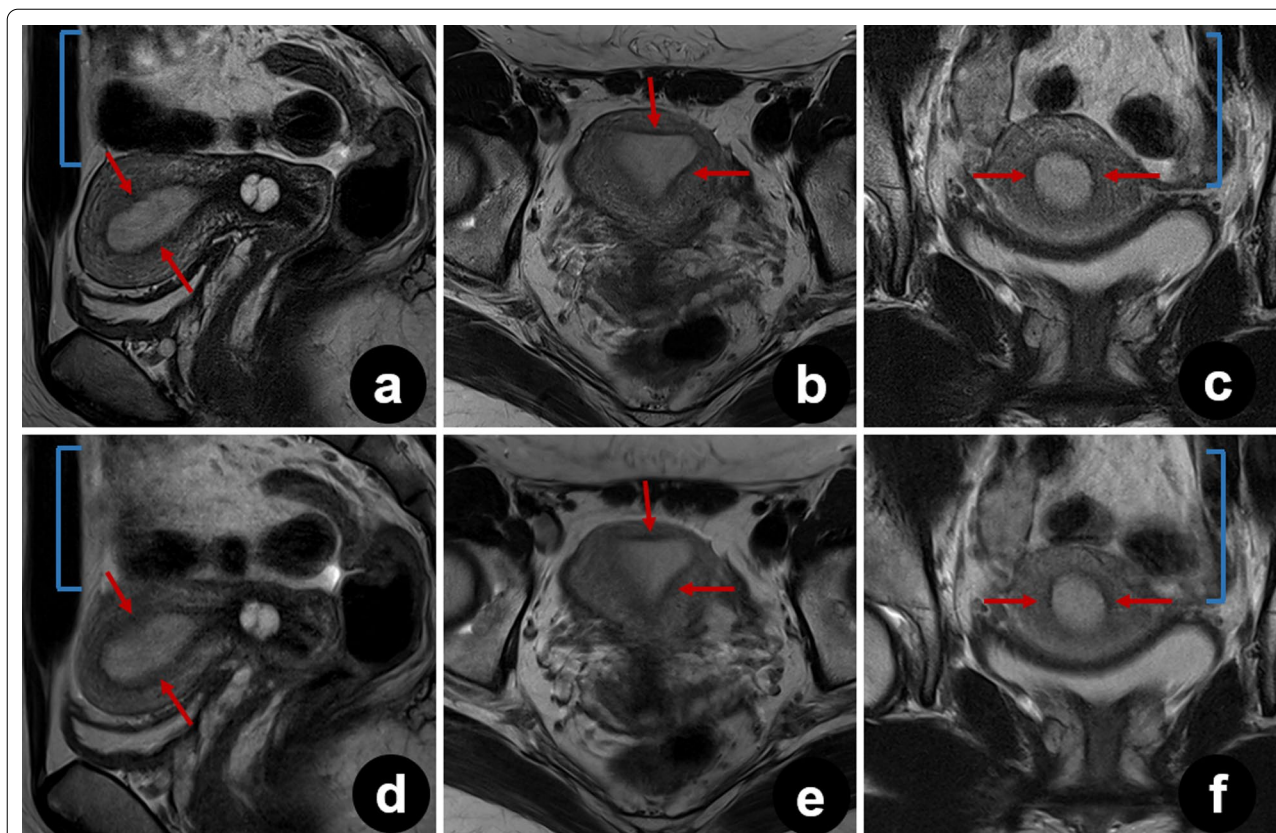


**Fig. 4** Pelvic T2<sub>DL</sub> and T2<sub>S</sub> images of a 25-year-old healthy female volunteer. **a–f** Sagittal (**a**), axial (**b**), and coronal (**c**) T2<sub>DL</sub> images and sagittal (**d**), axial (**e**), and coronal (**f**) T2<sub>S</sub> images. Fewer bowel peristalsis artifacts (brackets) were observed on T2<sub>DL</sub> images, which show sharper depiction of the uterine zonal layers (arrows). Due to severe motion artifacts (brackets), three uterine zonal layers were not clearly depicted on T2<sub>S</sub> images (arrows). T2<sub>DL</sub>, deep learning-accelerated T2-weighted turbo spin echo sequence; T2<sub>S</sub>, standard T2-weighted turbo spin echo sequence

and 6). In addition to a reduced amount of motion artifacts, T2<sub>DL</sub> images exhibited significantly higher conspicuity of the uterine zonal layers and lesions (Figs. 5 and 6). Scores for boundary sharpness of the zonal layers were significantly higher for T2<sub>DL</sub> than for T2<sub>S</sub>. Median (IQR) scores for T2<sub>DL</sub> and T2<sub>S</sub> were 5 (5–5) and 4 (4–5), 5 (4–5) and 4 (4–4), and 5 (4–5) and 4 (4–4), respectively in sagittal, axial, and coronal images (all  $p < 0.001$ ). Furthermore, lesion conspicuity was rated superior for T2<sub>DL</sub> compared with T2<sub>S</sub>, with a median (IQR) of 5 (4–5) versus 4 (4–4), respectively, for both sagittal and axial images and a median (IQR) of 5 (4–5) versus 4 (4–5) for coronal images ( $p = 0.002$ ,  $p < 0.001$ , and  $p = 0.021$ , respectively). The results of quantitative image evaluation of T2<sub>DL</sub> and T2<sub>S</sub> images by the three readers are presented in Table 4.

## Discussion

This prospective study first compared the feasibility of a T2<sub>DL</sub> with that of a T2<sub>S</sub> for gynecological MRI in healthy volunteers and patients with benign uterine disease. Compared to T2<sub>S</sub>, T2<sub>DL</sub> produced images with markedly

improved SNR and CNR without geometric distortion. Further, T2<sub>DL</sub> reduced the acquisition time by 62.7%. In addition, T2<sub>DL</sub> images displayed superior image quality, boundary sharpness of the uterine zonal layers, and lesion conspicuity of benign uterine disease, as well as fewer artifacts in the three planes.

In previous studies of the DL reconstruction technique for accelerated abdominal and prostate MR acquisitions, noise was subjectively rated as superior to that of standard sequence images [20, 24]. In the present study, the DL-accelerated technique was embedded in the female pelvic MRI protocol to acquire images for the first time. We designed to calculate the SNR and CNR values using the most commonly used measurement method (separate signal and noise regions in a single image), to objectively compare the image quality of T2<sub>DL</sub> and T2<sub>S</sub>. Some previously published studies revealed that such measurement method may degrade the SNR performance in parallel imaging, as noise is not evenly distributed in accelerated images reconstructed with parallel imaging [25, 26]. However, we aimed to compare the SNR

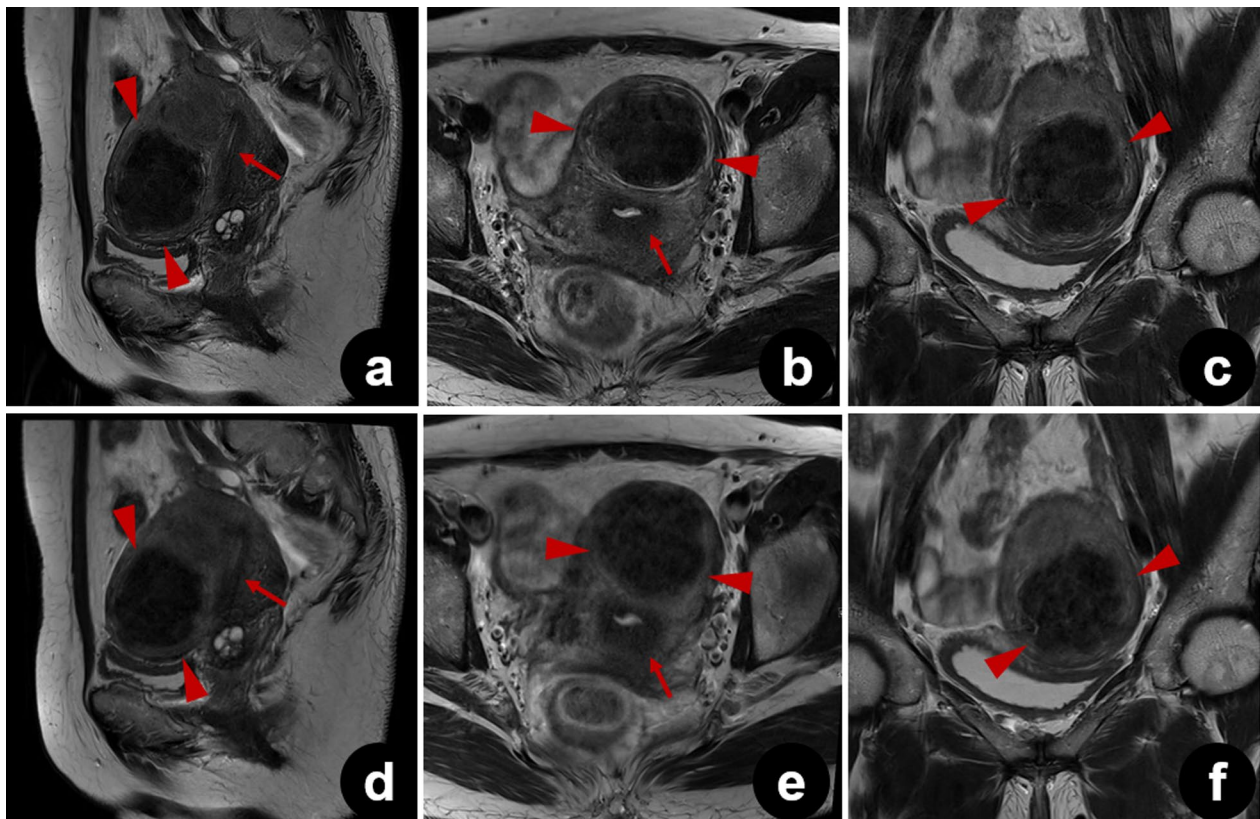


**Fig. 5** Pelvic  $T_{2_{DL}}$  and  $T_{2_S}$  images of a 47-year-old female patient with leiomyoma. **a–f** Sagittal (**a**), axial (**b**), and coronal (**c**)  $T_{2_{DL}}$  images and sagittal (**d**), axial (**e**), and coronal (**f**)  $T_{2_S}$  images. The edge and internal structure of the tumor were most clearly delineated by  $T_{2_{DL}}$  (between arrowheads). Note that sharper uterine zonal layers are also observed on  $T_{2_{DL}}$  images (arrows).  $T_{2_{DL}}$  deep learning-accelerated T2-weighted turbo spin echo sequence;  $T_{2_S}$  standard T2-weighted turbo spin echo sequence

and CNR values in two sequences ( $T_{2_{DL}}$  vs.  $T_{2_S}$ ) both with parallel imaging reconstruction, and the acquisition parameters, including repetition time, echo time, echo train length, and parallel acceleration factor used in  $T_{2_{DL}}$  are identical to those used in  $T_{2_S}$ . The ROIs on the image background were placed as large as possible (mean area: 1052.03 mm<sup>2</sup>) and were devoid of artifacts to reduce the impact of noise heterogeneity on the quantitative analysis. We found that although the mean SIs within the ROIs of the two sequences were similar in this study,  $T_{2_{DL}}$  images demonstrated considerably lower background noise intensity compared to  $T_{2_S}$  images. Therefore, the TSE sequence with DL reconstruction resulted in higher SNR and CNR values relative to the conventional approach. In addition, a higher CNR between the myometrium and junctional zone may have enhanced the boundary sharpness of the uterine zonal layers, as  $T_{2_{DL}}$  images were rated superior to  $T_{2_S}$  images on boundary sharpness evaluation by all three readers.

Motion artifacts pose a major challenge in pelvic MRI. Periodic motion from the lower anterior abdominal

wall and pulsatile vessels, as well as the random motion of the peristaltic viscera are key sources of artifact generation [27, 28]. The use of rapid image sequences may directly minimize random motion and facilitate breath-holding, thereby reducing motion artifacts [10, 11, 27]. Tsuboyama et al. reported that periodic motion produced marked ghost artifacts on conventional TSE, but not on half-Fourier acquisition single-shot turbo spin echo (HASTE) sequences, because the acquisition time was significantly shorter with HASTE than with TSE [29]. As shown in Fig. 4, bowel peristalsis and ghost artifacts were significantly reduced in  $T_{2_{DL}}$  images. Consequently, the effect of motion artifacts was smaller for  $T_{2_{DL}}$  than for  $T_{2_S}$ , resulting in more clearly delineated lesion edges and internal structures. Typical findings of adenomyosis, including poorly demarcated low-SI area, intramyometrial cysts, and small high-SI areas on T2W images, were more sharply depicted on  $T_{2_{DL}}$  than on  $T_{2_S}$ , as shown in Fig. 6 [30]. The finding that motion-robust  $T_{2_{DL}}$  images were evaluated as



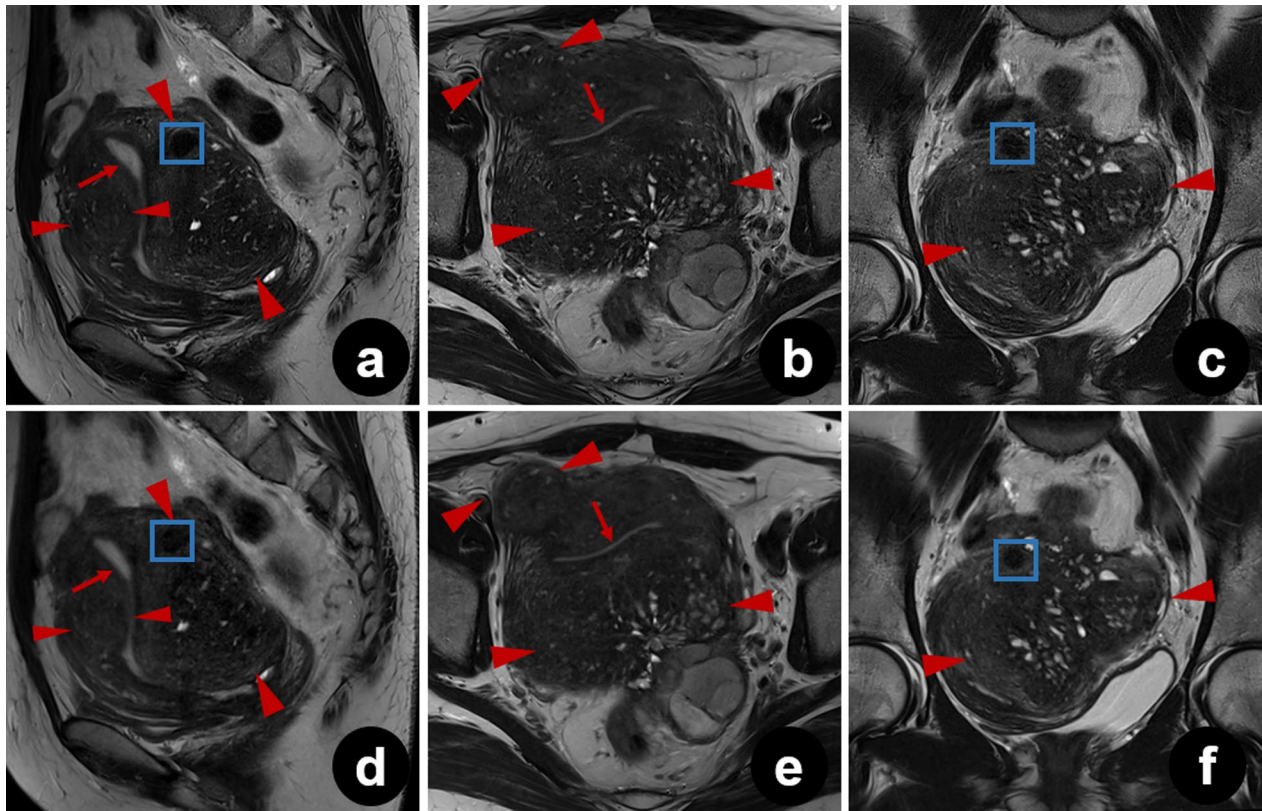


**Fig. 6** Pelvic  $T_{2DL}$  and  $T_{2S}$  images of a 43-year-old female patient with diffuse adenomyosis. Sagittal (a), axial (b), and coronal (c)  $T_{2DL}$  images and sagittal (d), axial (e), and coronal (f)  $T_{2S}$  images. Typical findings of asymmetry of uterine wall thickness, poorly demarcated low-SI area, and intramyometrial cysts are presented. Compared to  $T_{2S}$  images,  $T_{2DL}$  images exhibited greater conspicuity of the lesions (between arrowheads) and uterine zonal layers (arrows). Note that a small leiomyoma is also observed more clearly on sagittal and coronal  $T_{2DL}$  images (frame) than on the corresponding  $T_{2S}$  images. SI signal intensity;  $T_{2DL}$  deep learning-accelerated T2-weighted turbo spin echo sequence;  $T_{2S}$  standard T2-weighted turbo spin echo sequence

**Table 4** Qualitative image evaluations and inter-reader agreement for  $T_{2DL}$  and  $T_{2S}$  sequences

Characteristics	Reader 1			Reader 2			Reader 3			Kendall's W	
	$T_{2DL}$	$T_{2S}$	p values	$T_{2DL}$	$T_{2S}$	p values	$T_{2DL}$	$T_{2S}$	p values	$T_{2DL}$	$T_{2S}$
<i>Sagittal</i>											
Overall image quality	5 (4–5)	4 (4–5)	<0.001	5 (4–5)	4 (4–5)	<0.001	5 (4–5)	4 (4–5)	<0.001	0.873	0.887
Artifacts	5 (4–5)	4 (4–5)	<0.001	5 (4–5)	4 (4–5)	<0.001	5 (4–5)	4 (4–5)	<0.001	0.903	0.914
Boundary sharpness	5 (4–5)	4 (4–5)	<0.001	5 (4–5)	4 (4–5)	<0.001	5 (5–5)	4 (4–5)	<0.001	0.801	0.771
Lesion conspicuity	5 (5–5)	4 (4–4)	<0.001	5 (4–5)	4 (4–4)	<0.001	5 (4–5)	4 (4–4)	0.002	0.847	0.871
<i>Axial</i>											
Overall image quality	5 (4–5)	4 (4–4)	<0.001	5 (4–5)	4 (4–4)	<0.001	5 (4–5)	4 (4–4)	<0.001	0.851	0.871
Artifacts	5 (4–5)	4 (4–4)	<0.001	5 (4–5)	4 (4–4)	<0.001	5 (5–5)	4 (4–5)	<0.001	0.840	0.828
Boundary sharpness	5 (4–5)	4 (4–4)	<0.001	5 (4–5)	4 (4–4)	<0.001	5 (4–5)	4 (4–4)	<0.001	0.828	0.841
Lesion conspicuity	5 (4–5)	4 (4–4)	<0.001	5 (5–5)	4 (4–4)	<0.001	5 (4–5)	4 (4–4)	<0.001	0.896	0.884
<i>Coronal</i>											
Overall image quality	5 (4–5)	4 (4–4)	<0.001	5 (4–5)	4 (4–4)	<0.001	5 (4–5)	4 (4–4)	<0.001	0.867	0.905
Artifacts	5 (4–5)	4 (4–5)	<0.001	5 (4–5)	4 (4–4)	<0.001	5 (4–5)	4 (4–5)	<0.001	0.876	0.890
Boundary sharpness	5 (4–5)	4 (4–4)	<0.001	5 (4–5)	4 (4–4)	<0.001	5 (4–5)	4 (4–4)	<0.001	0.903	0.882
Lesion conspicuity	5 (4–5)	4 (4–4)	0.001	5 (4–5)	4 (4–4)	0.003	5 (4–5)	4 (4–5)	0.021	0.864	0.879

$T_{2DL}$  deep learning-accelerated T2-weighted turbo spin echo sequence;  $T_{2S}$  standard T2-weighted turbo spin echo sequence

superior to T2<sub>S</sub> images suggests that these accelerated images may be clinically acceptable.

Gynecological MRI has been recognized as the optimal imaging modality for the assessment of pelvic diseases in women. Accordingly, the DL reconstruction technique, which accelerates gynecological imaging, offers relevant clinical benefits [2, 29, 31]. The shorter sequencing time may reduce MRI costs and permit greater patient throughput and/or more imaging to be completed per unit time. Furthermore, fast imaging sequences may relieve patient anxiety, thereby allowing the acquisition of motion-robust images with optimal diagnostic value. In future, the accelerated gynecological MRI protocol may be harnessed as a candidate or even a replacement for conventional protocols.

This study has several limitations. First, as the study involved preliminary experiments using a DL reconstruction technique for gynecological MRI, the study population was small and was derived from a single center. Future multicenter studies involving larger cohorts are needed to evaluate the robustness and diagnostic ability of T2<sub>DL</sub> images. Second, since varying noise distributions resulting from the deployed neural networks may exist, the validity of the SNR and CNR measurement in the present study is not clear. Measurement methods applicable for MR images with the DL reconstruction should be proposed for quantitative evaluation in future studies. Third, patients we included had different benign lesion types, which could potentially affect subjective and objective analyses. Future studies involving patients with the same lesion type are recommended. Finally, the conclusions may have limited generalizability, because only healthy volunteers and patients with benign uterine diseases were enrolled. The image quality and diagnostic performance of T2<sub>DL</sub> images in women with other pelvic diseases, especially gynecologic malignancies, remain to be elucidated. In this regard, the clinical value of this DL reconstruction technique should be further explored for other gynecological diseases.

In conclusion, the DL-accelerated T2w TSE sequence is an effective and promising approach that reduces the acquisition time of female pelvic MRI compared to the standard TSE sequence, with the added benefits of significantly improved image quality, boundary sharpness, and lesion conspicuity in patients with benign uterine disease.

#### Abbreviations

CNR: Contrast-to-noise ratio; CS: Compressed sensing; DL: Deep learning; IQR: Interquartile range; SD: Standard deviation; SI: Signal intensity; SNR: Signal-to-noise ratio; T2<sub>DL</sub>: Deep learning-accelerated T2-weighted turbo spin echo sequence; T2<sub>S</sub>: Standard T2-weighted turbo spin echo sequence; T2W: T2-weighted imaging; TSE: Turbo spin echo.

#### Acknowledgments

The authors extend gratitude to support grants from Natural Science Foundation of China (Grant No. 81901829), National High Level Hospital Clinical Research Funding (Grant Nos. 2022-PUMCH-A-004 & 2022-PUMCH-A-109).

#### Author contributions

Y-LH, H-DX, Z-YJ: conceptualization; Y-LH: Funding acquisition; JR, YL: formal analysis; JR: data curation; F-SL, CL, J-XZ: investigation; MDN, X-YW: validation; JZ, X-YL: software; JR: writing—original draft; YL, Y-LH, H-DX, Z-YJ: writing—review.

#### Funding

This work was supported by grants from Natural Science Foundation of China (GrantNo. 81901829), National High Level Hospital Clinical Research Funding (Grant Nos.2022-PUMCH-A-004 & 2022-PUMCH-A-109).

#### Availability of data and materials

The datasets analyzed during the current study are available from the corresponding author on reasonable request.

#### Declarations

##### Ethics approval and consent to participate

This prospective study was approved by our institutional review board and complied with ethical committee standards. Written informed consent was obtained from participants.

##### Consent for publication

Not applicable.

##### Competing interests

Co-author Jin-Xia Zhu and Xiao-Ye Wang are employees of Siemens Healthineers Ltd., Beijing, China and Marcel Dominik Nickel is an employee of Siemens Healthcare GmbH, Erlangen, Germany. The other authors have no conflicts of interest to disclose. The authors not employed by Siemens were in control of this study.

##### Author details

<sup>1</sup>Department of Radiology, Peking Union Medical College Hospital, Chinese Academy of Medical Sciences and Peking Union Medical College, Shuai Fu Yuan Road, Dongcheng Dist., Beijing 100730, People's Republic of China.

<sup>2</sup>Department of Obstetrics and Gynecology, Peking Union Medical College Hospital, Chinese Academy of Medical Sciences and Peking Union Medical College, National Clinical Research Center for Obstetric and Gynecologic Diseases, Beijing, People's Republic of China. <sup>3</sup>MR Collaboration, Siemens Healthineers Ltd., Beijing, People's Republic of China. <sup>4</sup>MR Application Predevelopment, Siemens Healthcare GmbH, Erlangen, Germany. <sup>5</sup>MR Clinical Marketing, Siemens Healthineers Ltd., Beijing, People's Republic of China.

Received: 16 May 2022 Accepted: 29 October 2022

Published online: 13 December 2022

#### References

- Bazot M, Bharwani N, Huchon C et al (2017) European society of urogenital radiology (ESUR) guidelines: MR imaging of pelvic endometriosis. *Eur Radiol* 27:2765–2775. <https://doi.org/10.1007/s00330-016-4673-z>
- Nougaret S, Horta M, Sala E et al (2019) Endometrial cancer MRI staging: Updated Guidelines of the European Society of Urogenital Radiology. *Eur Radiol* 29:792–805. <https://doi.org/10.1007/s00330-018-5515-y>
- Balcacer P, Shergill A, Litkouhi B (2019) MRI of cervical cancer with a surgical perspective: staging, prognostic implications and pitfalls. *Abdom Radiol (NY)* 44:2557–2571. <https://doi.org/10.1007/s00261-019-01984-7>
- Manganaro L, Lakhman Y, Bharwani N et al (2021) Staging, recurrence and follow-up of uterine cervical cancer using MRI: Updated Guidelines of the European Society of Urogenital Radiology after revised FIGO staging 2018. *Eur Radiol*. <https://doi.org/10.1007/s00330-020-07632-9>
- Balleyguier C, Sala E, Da Cunha T et al (2011) Staging of uterine cervical cancer with MRI: guidelines of the European Society of

- Urogenital Radiology. *Eur Radiol* 21:1102–1110. <https://doi.org/10.1007/s00330-010-1998-x>
6. Foti PV, Farina R, Palmucci S et al (2018) Endometriosis: clinical features, MR imaging findings and pathologic correlation. *Insights Imaging* 9:149–172. <https://doi.org/10.1007/s13244-017-0591-0>
  7. Zhang Q, Ouyang H, Ye F et al (2021) Feasibility of intravoxel incoherent motion diffusion-weighted imaging in distinguishing adenocarcinoma originated from uterine corpus or cervix. *Abdom Radiol (NY)* 46:732–744. <https://doi.org/10.1007/s00261-020-02586-4>
  8. Qi YF, He YL, Lin CY et al (2020) Diffusion-weighted imaging of cervical cancer: Feasibility of ultra-high b-value at 3T. *Eur J Radiol* 124:108779. <https://doi.org/10.1016/j.ejrad.2019.108779>
  9. Vanderby S, Badea A, Peña Sánchez JN, Kalra N, Babyn P (2017) Variations in magnetic resonance imaging provision and processes among Canadian academic centres. *Can Assoc Radiol J* 68:56–65. <https://doi.org/10.1016/j.carj.2016.07.007>
  10. Stadler A, Schima W, Ba-Ssalamah A, Kettenbach J, Eisenhuber E (2007) Artifacts in body MR imaging: their appearance and how to eliminate them. *Eur Radiol* 17:1242–1255. <https://doi.org/10.1007/s00330-006-0470-4>
  11. Yang RK, Roth CG, Ward RJ, deJesus JO, Mitchell DG (2010) Optimizing abdominal MR imaging: approaches to common problems. *Radiographics* 30:185–199. <https://doi.org/10.1148/rg.301095076>
  12. Griswold MA, Jakob PM, Heidemann RM et al (2002) Generalized auto-calibrating partially parallel acquisitions (GRAPPA). *Magn Reson Med* 47:1202–1210. <https://doi.org/10.1002/mrm.10171>
  13. Hollingsworth KG (2015) Reducing acquisition time in clinical MRI by data undersampling and compressed sensing reconstruction. *Phys Med Biol* 60:R297–322. <https://doi.org/10.1088/0031-9155/60/21/r297>
  14. Lustig M, Donoho D, Pauly JM (2007) Sparse MRI: The application of compressed sensing for rapid MR imaging. *Magn Reson Med* 58:1182–1195. <https://doi.org/10.1002/mrm.21391>
  15. Jaspán ON, Fleysher R, Lipton ML (2015) Compressed sensing MRI: a review of the clinical literature. *Br J Radiol* 88:20150487. <https://doi.org/10.1259/bjr.20150487>
  16. Hammernik K, Klatzer T, Kobler E et al (2018) Learning a variational network for reconstruction of accelerated MRI data. *Magn Reson Med* 79:3055–3071. <https://doi.org/10.1002/mrm.26977>
  17. Gassenmaier S, Afat S, Nickel MD et al (2021) Accelerated T2-weighted TSE imaging of the prostate using deep learning image reconstruction: a prospective comparison with standard T2-weighted TSE imaging. *Cancers*. <https://doi.org/10.3390/cancers13143593>
  18. Herrmann J, Gassenmaier S, Nickel D et al (2021) Diagnostic confidence and feasibility of a deep learning accelerated Haste sequence of the abdomen in a single breath-hold. *Invest Radiol* 56:313–319. <https://doi.org/10.1097/rli.0000000000000743>
  19. Recht MP, Zbontar J, Sodickson DK et al (2020) Using deep learning to accelerate knee MRI at 3 T: results of an interchangeability study. *AJR Am J Roentgenol* 215:1421–1429. <https://doi.org/10.2214/ajr.20.23313>
  20. Gassenmaier S, Afat S, Nickel D, Mostapha M, Herrmann J, Othman AE (2021) Deep learning-accelerated T2-weighted imaging of the prostate: reduction of acquisition time and improvement of image quality. *Eur J Radiol* 137:109600. <https://doi.org/10.1016/j.ejrad.2021.109600>
  21. He YL, Ding N, Qi YF et al (2019) Visualising the boundary sharpness of uterine zonal structures using high-resolution T2-weighted images during the menstrual cycle. *Clin Radiol* 74:81.e19–81.e24. <https://doi.org/10.1016/j.crad.2018.09.008>
  22. Badachhane AA, Kumar A, Ghaghada KB et al (2019) Pre-clinical magnetic resonance imaging of retroplacental clear space throughout gestation. *Placenta* 77:1–7. <https://doi.org/10.1016/j.placenta.2019.01.017>
  23. Hossein J, Fariborz F, Mehrnaz R, Babak R (2019) Evaluation of diagnostic value and T2-weighted three-dimensional isotropic turbo spin-echo (3D-SPACE) image quality in comparison with T2-weighted two-dimensional turbo spin-echo (2D-TSE) sequences in lumbar spine MR imaging. *Eur J Radiol Open* 6:36–41. <https://doi.org/10.1016/j.ejro.2018.12.003>
  24. Herrmann J, Nickel D, Mugler JP et al (2021) Development and evaluation of deep learning-accelerated single-breath-hold abdominal Haste at 3 T using variable refocusing flip angles. *Invest Radiol* 56:645–652. <https://doi.org/10.1097/rli.0000000000000785>
  25. Dietrich O, Raya JG, Reeder SB, Reiser MF, Schoenberg SO (2007) Measurement of signal-to-noise ratios in MR images: influence of multichannel coils, parallel imaging, and reconstruction filters. *J Magn Reson Imaging* 26:375–385. <https://doi.org/10.1002/jmri.20969>
  26. Heverhagen JT (2007) Noise measurement and estimation in MR imaging experiments. *Radiology* 245:638–639. <https://doi.org/10.1148/radiol.2453062151>
  27. Zand KR, Reinhold C, Haider MA, Nakai A, Rohoman L, Maheshwari S (2007) Artifacts and pitfalls in MR imaging of the pelvis. *J Magn Reson Imaging* 26:480–497. <https://doi.org/10.1002/jmri.20996>
  28. Zaitsev M, Maclaren J, Herbst M (2015) Motion artifacts in MRI: a complex problem with many partial solutions. *J Magn Reson Imaging* 42:887–901. <https://doi.org/10.1002/jmri.24850>
  29. Tsuboyama T, Takei O, Okada A, Honda T, Kuriyama K (2020) Comparison of HASTE with multiple signal averaging versus conventional turbo spin echo sequence: a new option for T2-weighted MRI of the female pelvis. *Eur Radiol* 30:3245–3253. <https://doi.org/10.1007/s00330-020-06686-z>
  30. Chapron C, Vannuccini S, Santulli P et al (2020) Diagnosing adenomyosis: an integrated clinical and imaging approach. *Hum Reprod Update* 26:392–411. <https://doi.org/10.1093/humupd/dmz049>
  31. Khan SR, Arshad M, Wallitt K, Stewart V, Bharwani N, Barwick TD (2017) What's new in imaging for gynecologic cancer? *Curr Oncol Rep* 19:85. <https://doi.org/10.1007/s11912-017-0640-3>

## Publisher's Note

Springer Nature remains neutral with regard to jurisdictional claims in published maps and institutional affiliations.

Submit your manuscript to a SpringerOpen® journal and benefit from:

- Convenient online submission
- Rigorous peer review
- Open access: articles freely available online
- High visibility within the field
- Retaining the copyright to your article

Submit your next manuscript at ► [springeropen.com](https://www.springeropen.com)